International Journal of Machine Tools & Manufacture 51 (2011) 309–319

Contents lists available at ScienceDirect

International Journal of Machine Tools & Manufacture

journal homepage: www.elsevier.com/locate/ijmactool

Realisation of grinding-hardening in workpieces of curved surfaces—Part 1: Plunge cylindrical grinding

Thai Nguyen *, L.C. Zhang

School of Mechanical and Manufacturing Engineering, The University of New South Wales, NSW 2052, Australia

ARTICLE INFO

Article history:
Received 8 September 2010
Received in revised form
10 December 2010
Accepted 13 December 2010
Available online 21 December 2010

Keywords:
Grinding–hardening
Plunge cylindrical grinding
Temperature field
Hardened layer thickness
Variation of depth of cut

ABSTRACT

This paper investigates the feasibility to achieve grinding-hardening in a plunge cylindrical grinding process. To understand the mechanisms, a temperature-dependent finite element heat transfer model incorporating a triangular moving heat source was developed to describe the temperature field, thus to predict the thickness of the grinding-hardened layer. The analysis carried out included the variation effect of depth of cut caused by the change in wheel–workpiece engagement. The model was applied on quenchable steel 1045 and the analysis was verified experimentally. It was shown that the heating cycle in plunge cylindrical grinding is the result of consecutive heating and cooling processes, varying from location to location in a workpiece. The ratio of the workpiece speed to the infeed rate plays an important role in the heat treatment cycle.

1. Introduction

Grinding–hardening is a technology that uses the heat generated in grinding to create a hardened surface layer by promoting the phase transformation in quenchable steel components [1–3]. Metallurgical studies on the layer hardened by this method have shown an enhancement of dislocations and carbon distribution compared to that by conventional quenching, resulted in a remarkable improvement in the resistance of wear and fatigue of the material [2,4,5].

The kinetics of phase transformations in steel depends greatly on temperature and time during a heat treatment process [6]. Unlike conventional heat treatment methods where the heating and quenching cycles can be relatively easily controlled, thermal cycle in grinding is complex. The grinding heat source, approximately triangular [7,8], is generated within a small wheel–workpiece contact zone. Depending on the grinding operations, this heat source moves on the grinding surface in different trajectories. In plunge cylindrical grinding, the heat source sweeps over the cylindrical surface of a workpiece due to the rotation of the workpiece about its axis and the radial feed of the grinding wheel. The continuous radial feed of the grinding wheel changes the wheel's instant depth of cut when the workpiece rotates. Because of such instant change in the depth of cut, the intensity of the heat source generated by grinding varies. Since this heat source is moving along the workpiece surface, materials at different locations experience different heat conduction and convection processes [9,10], leading to a variation of the thickness and microstructure of the grinding-hardened layer. The heat transfer analysis of grinding to date is limited to two-dimensional cases and to surface grinding [11].

This paper aims to investigate the feasibility of grinding-hardening in a plunge cylindrical grinding process. The study will first establish a temperature-dependent, three-dimensional (3D) heat transfer model with the aid of the finite element method to explore the temperature field during the process and hence to predict the thickness of the hardened layer. Relevant experiment will then be carried out to verify the theoretical prediction.

2. Modelling

2.1. Thermal analysis

Fig. 1 illustrates the schematic diagram of heat transfer during the grinding of a cylindrical workpiece. The calculation of the temperature field is based on an unsteady-state heat conduction equation [12]:

$$\frac{1}{r}\frac{\partial}{\partial r}\left(kr\frac{\partial T}{\partial r}\right)+\frac{1}{r^2}\frac{\partial}{\partial \theta}\left(k\frac{\partial T}{\partial \theta}\right)+\frac{\partial}{\partial z}\left(k\frac{\partial T}{\partial z}\right)+\dot{q}=\frac{1}{\alpha}\frac{\partial T}{\partial t} \quad (1)$$

in which $\dot{q}$ is the heat rate per unit volume generated during phase transformation, k is the thermal conductivity, $\alpha=k/\rho C_p$ is the thermal diffusivity, where ρ is the density and C_P is the specific heat.

* Corresponding author. Tel.: +61 2 9385 5689; fax: +61 2 9663 1222.
E-mail address: thai.nguyen@unsw.edu.au (T. Nguyen).

0890-6955/$ - see front matter Crown Copyright © 2010 Published by Elsevier Ltd. All rights reserved.
doi:10.1016/j.ijmachtools.2010.12.006

Nomenclature

A_o	average single grain-workpiece contact area, m^2
a	actual depth of cut, m
B	width ground, m
C_P	specific heat, $J\,kg^{-1}\,K^{-1}$
d_{eq}	equivalent wheel diameter, m
d_g	wheel grain size, m
f	controlled infeed, m
f_d	designed total infeed, m
f_p	volume fraction of phase p
G_a	number of active grains per unit area of the wheel surface
h	heat transfer coefficient, $W\,m^{-2}K^{-1}$
I	number of workpiece rotations required to complete the operation
k	thermal conductivity of workpiece, $Wm^{-1}\,K^{-1}$
l_c	wheel–workpiece contact arc length, m
M	manufacturing grit number
N	number of divisions equally divided on the workpiece circumference
Nu	Nusselt number
$\vec{n}$	vector normal to the surface of a boundary
R_s	grinding wheel radius, m
R_w	initial workpiece radius, m
Re	Reynolds number
Pr	Prandtl number
$\dot{q}$	heat rate per unit volume during phase transformation, Wm^{-3}
q_c	heat flux due to convection, $W\,m^{-2}$
q_p	peak on a triangle grinding heat flux profile, $W\,m^{-2}$
q_r	heat flux due to radiation, $W\,m^{-2}$
$\overline{q}$	average grinding heat flux, $W\,m^{-2}$
r	actual infeed, m
T	temperature, K or $^\circ C$
T_f	film temperature (T_f=0.5(T_w+T_a)), K or $^\circ C$
T_s	surface temperature, K or $^\circ C$
T_∞	ambient temperature, K or $^\circ C$
T_o	time for a heat source moves over the distance of a contact length, s
t	time, s
t_o	time for a heat source moves over the distance of a unit length, s
u	controlled infeed rate, $m\,s^{-1}$
u_g	specific grinding energy, $J\,m^{-3}$
$\dot{V}$	specific material removal rate per unit wheel width, $m^3(m\,s)^{-1}$
V_p	volumetric packaging density of grains in the wheel constituent
v	actual infeed rate, $m\,s^{-1}$
v_s	wheel speed, $m\,s^{-1}$
v_w	workpiece speed, $m\,s^{-1}$
ΔH_p	enthalpy of transformation from austenite to phase p, $J\,kg^{-1}$
γ	abrasive shape factor
δ	probed thickness of hardened layer, m
Δ	actual thickness of hardened layer, m
ε	emissivity
η	heat partition ratio, %
θ_c	angle of the wheel-work contact on the workpiece, rad
θ_d	angle associated with the designed total infeed (f_d), rad
τ	characteristic time constant of a grinding system, s
υ	air viscosity, $m^2\,s^{-1}$
ρ	workpiece density, $kg\,m^{-3}$
σ	Stefan–Boltzmann constant, ($\sigma=5.67\times10^{-8}\,Wm^{-2}\,K^{-4}$)
ω_s	rotational speed of the grinding wheel, $rad\,s^{-1}$
ω_w	rotational speed of the workpiece, $rad\,s^{-1}$
(r, θ, z)	cylindrical coordinate system

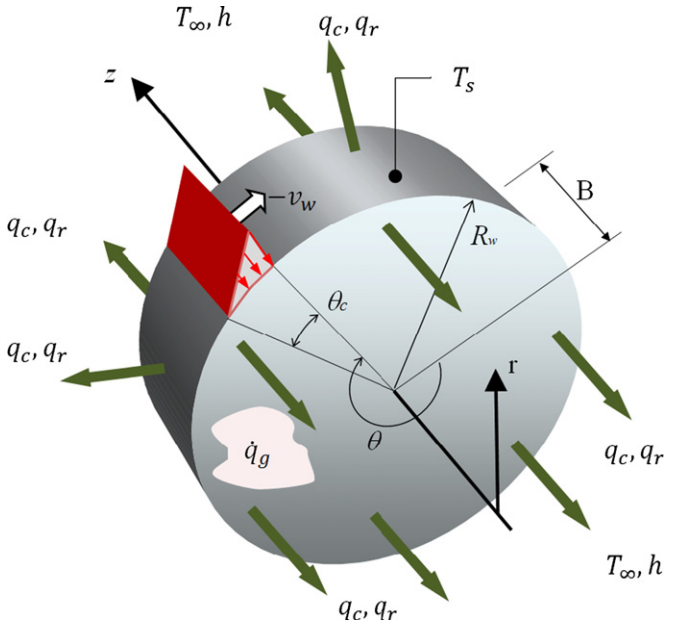

Fig. 1. Conduction in the workpiece during plunge cylindrical grinding.

During phase transformation, there is an associated change in enthalpy. In a quenching process, the microstructure of steel is assumed to be a mixture of austenite, ferrite, pearlite, bainite and martensite. The linear law of mixture is adopted to which $\dot{q}$ can be derived as [13]

$$\dot{q} = \frac{\rho}{\Delta t}\sum_{p=2}^{5}\frac{\partial \Delta H_p}{\partial f_p}df_p \tag{2}$$

where f_p is the volume percentage of phase p and ΔH_p, the enthalpy of transformation, is taken as 75.2, 92.0, 92.0 and 83.6 kJ kg^{-1} for austenite→ferrite, austenite→pearlite, austenite→bainite and austenite→martensite reactions, respectively [13]. The volume percentage of phase p (f_p), according to the continuous cooling transformation (CCT) diagram, depends on the cooling rate of the process, which follows two kinds of phase transformation kinetics: diffusion controlled transformation and martensitic transformation [14–16]. The details of calculating f_p can be found in Ref. [11].

The thermal properties (k, ρ and C_P) of the workpiece material (steel 1045) are temperature-dependant, which are accommodated in the finite element computation using ANSYS, have been presented in Ref. [11].

Eq. (1) can be solved by subjecting it to the initial and boundary conditions as described below:

2.1.1. Initial conditions

$$T_\infty = 22\,^\circ\mathrm{C}\ \text{(constant ambient temperature)} \tag{3}$$

$$T(r,t)\big|_{t=0} = T_\infty, \quad 0 \le r \le R_w \tag{4}$$

where R_w is the initial radius of the workpiece cylinder.

2.1.2. Boundary conditions for heating by the moving heat source

The surface heat flux due to grinding can be viewed as a heat source gliding on the workpiece surface with the same velocity as the tangential velocity of the workpiece but in opposite direction, i.e., $-v_w$. In plunge grinding, the heat source has a constant width (B), which is equal to the width of the grinding wheel. For an up grinding, the distribution of the heat flux can be approximated as a triangle [3,7,8], having a linear distribution over the wheel–workpiece contact arc, l_c, and can be expressed as

$$q(l)|_{t=const} = q_p - \frac{q_p}{l_c}|l|, \quad l \in l_c \tag{5}$$

where q_p is the peak heat flux, determined by

$$\overline{q} = \frac{1}{l_c}\int_0^{l_c} q(l)dl = 0.5q_p \tag{6}$$

The average surface heat flux ($\overline{q}$) is determined by

$$\overline{q} = \eta\frac{u_g\dot{V}}{l_c} \tag{7}$$

where u_g is the specific grinding energy obtained from experiments [17–19] (see Appendix A1), η is the fraction of total energy conducted as heat into the workpiece (heat partition ratio; see Appendix A2), and $\dot{V}$ is the specific material removal rate per unit wheel width, which is determined by [17]:

$$\dot{V} = v_w a\frac{(2R_w - a)}{2(R_w - a)} \tag{8}$$

At an instance depth of cut (a), the length of the wheel–workpiece contact arc (l_c) is determined by [20]

$$l_c \approx \sqrt{ad_{eq}} \tag{9}$$

where d_{eq} is the equivalent wheel diameter, defined as

$$d_{eq} = \frac{2R_s}{1 + R_s/(R_w - a)} \tag{10}$$

in which R_s is the grinding wheel radius.

When using ANSYS to solve the problem, the workpiece was meshed by dividing its circumference surface with N equal elements. The heat flux variation with respect to the time applied on the nth element can be derived as:

$$q(n,t) = \begin{cases} q_p\left(1 - \frac{t-(n-1)t_0}{T}\right), & (n-1)t_0 \le t \le (n-1)t_0 + T_0 \\ 0, & t < (n-1)t_0 \cup t > (n-1)t_0 + T_0 \end{cases} \tag{11}$$

where $t_0 = (2\pi R_w)/(Nv_w)$ and $T_0 = l_c/v_w$ are the time intervals that the heat source spends to move over the distances of a unit length and of the contact length, respectively.

2.1.3. Cooling conditions

The Neumann boundary conditions for cooling can be described as

$$-k\frac{\partial T}{\partial \vec{n}} = q_c + q_r = h(T_s - T_\infty) + \varepsilon\sigma(T_s^4 - T_\infty^4) \tag{12}$$

where $\vec{n}$ is the unit vector normal to the surface of a boundary, q_c and q_r are the surface heat fluxes associated with the convective cooling and radiation, respectively, h is the heat transfer coefficient applied to the boundary surface, T_s is the surface temperature, σ is the Stefan–Boltzmann constant ($5.67 \times 10^{-8}\ \mathrm{Wm^{-2}\,K^{-4}}$) and ε is the emissivity of the workpiece material ($\varepsilon = 0.21$ [12]).

On the surface normal to the two sides of the workpiece cylinder ($\vec{n}_z$ and $-\vec{n}_z$),

$$h|_{z=0} = h|_{z=B} = h_a \tag{13}$$

and

$$q_r|_{z=0} = q_r|_{z=B} = \varepsilon\sigma(T_s^4 - T_\infty^4) \tag{14}$$

where h_a is the heat transfer coefficient due to air flow, determined in Appendix A3.

However, on the circumferential surface of the workpiece where the grinding heat flux is applied, only the area outside the grinding zone is subjected to convective cooling and radiation. The heat transfer coefficient is

$$h(\theta)|_{r=R_w} = \begin{cases} 0, & \theta \in \theta_c \quad \text{(within the griding zone)} \\ h_a, & \theta \overline{\in} \theta_c \quad \text{(outside the griding zone)} \end{cases} \tag{15}$$

and the radiation heat flux is

$$q_r|_{r=R_w} = \begin{cases} 0, & \theta \in \theta_c \text{(within the griding zone)} \\ \varepsilon\sigma(T_s^4 - T_\infty^4), & \theta \overline{\in} \theta_c \text{(outside the griding zone)} \end{cases} \tag{16}$$

where θ_c is the wheel–workpiece contact angle (Fig. 1) and since θ_c is small,

$$\theta_c \approx \frac{l_c}{R_w} \tag{17}$$

2.2. Depth of cut

In plunge cylindrical grinding, as illustrated in Fig. 2, the depth of cut varies during the machining operation. This change influences significantly the temperature variation in the workpiece material, and in turn, affects the possible phase transformation events for grinding-hardening. Thus to explore the temperature field evolution, it is necessary to integrate the change of the depth of cut into the thermal analysis.

The workpiece follows two controlled motions. One is the rotation about the workpiece axis with an angular velocity (ω_w)

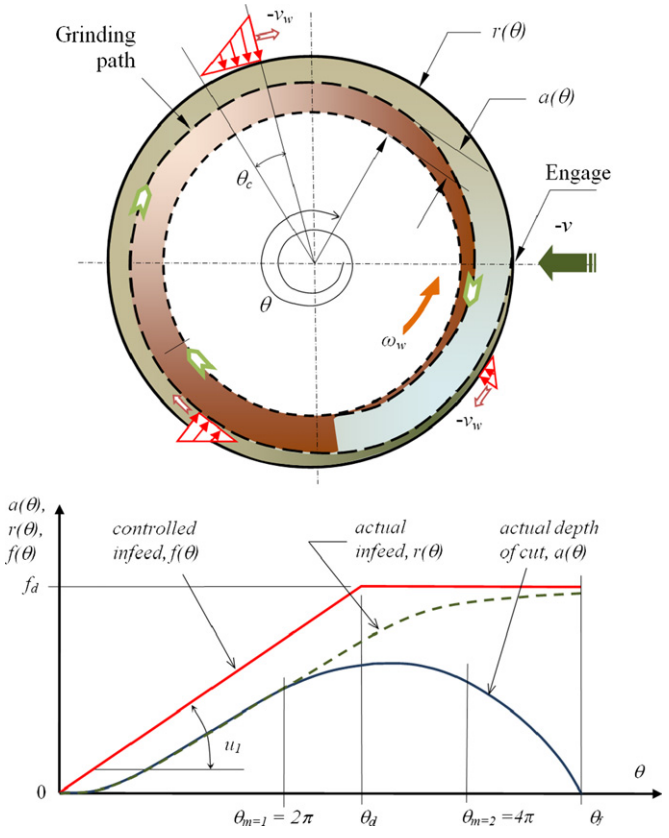

Fig. 2. Variation of depth of cut in plunge cylindrical grinding.

and the other is an infeed motion along the direction along the centres of the workpiece and the grinding wheel. This motion has a controlled infeed rate of $u(t)$. The equations of these controlled motions can be described as

$$\begin{cases} \theta(t) = \omega_w t \\ f(t) = \int_o^t u(t)dt \end{cases} \quad (18a, b)$$

where $\theta(t)$ and $f(t)$ are the angular position and the total controlled infeed at time instant t, respectively.

To ensure a largest possibility of grinding heating, the controlled infeed rate u was maintained during the operation until reaching the designed total infeed (f_d), by passing the finish stage [21], i.e.

$$\begin{cases} u(t) = u_1 = const, \quad t \le t_1 = f_d/u_1 \\ u(t) = 0, \quad t > t_1 \end{cases} \quad (19a, b)$$

However, because of the deflection of the grinding system, the actual infeed rate ($v(t)$) corresponding to the reduction in radial dimension of the workpiece is less than the controlled infeed rate ($u(t)$) of the machine. The dynamics of the system can be described as [22]:

$$\dot{v}(t) = \frac{1}{\tau}[u(t) - v(t)] \quad (20)$$

where τ denotes the characteristic time constant of a grinding system. For external grinding, a typical constant τ varies from 0.5 to 1.0 s [23]. In this study, under external grinding using short wheel spindle and with two end stiffness supports for a relatively short workpiece shaft (90 mm in length and moment of inertia of 7.9×10^3 mm^4), τ is taken as 0.5 s.

Solving Eq. (20) gives

(a) For the first stage of ($t \le t_1$) in associated with the engagement ($\theta \le \theta_d = \omega_w f_d/u_1$) where $u(t) = u_1$, the initial condition is $v(0) = 0$ to which

$$v_1(t) = u_1[1 - e^{-t/\tau}] \quad (21)$$

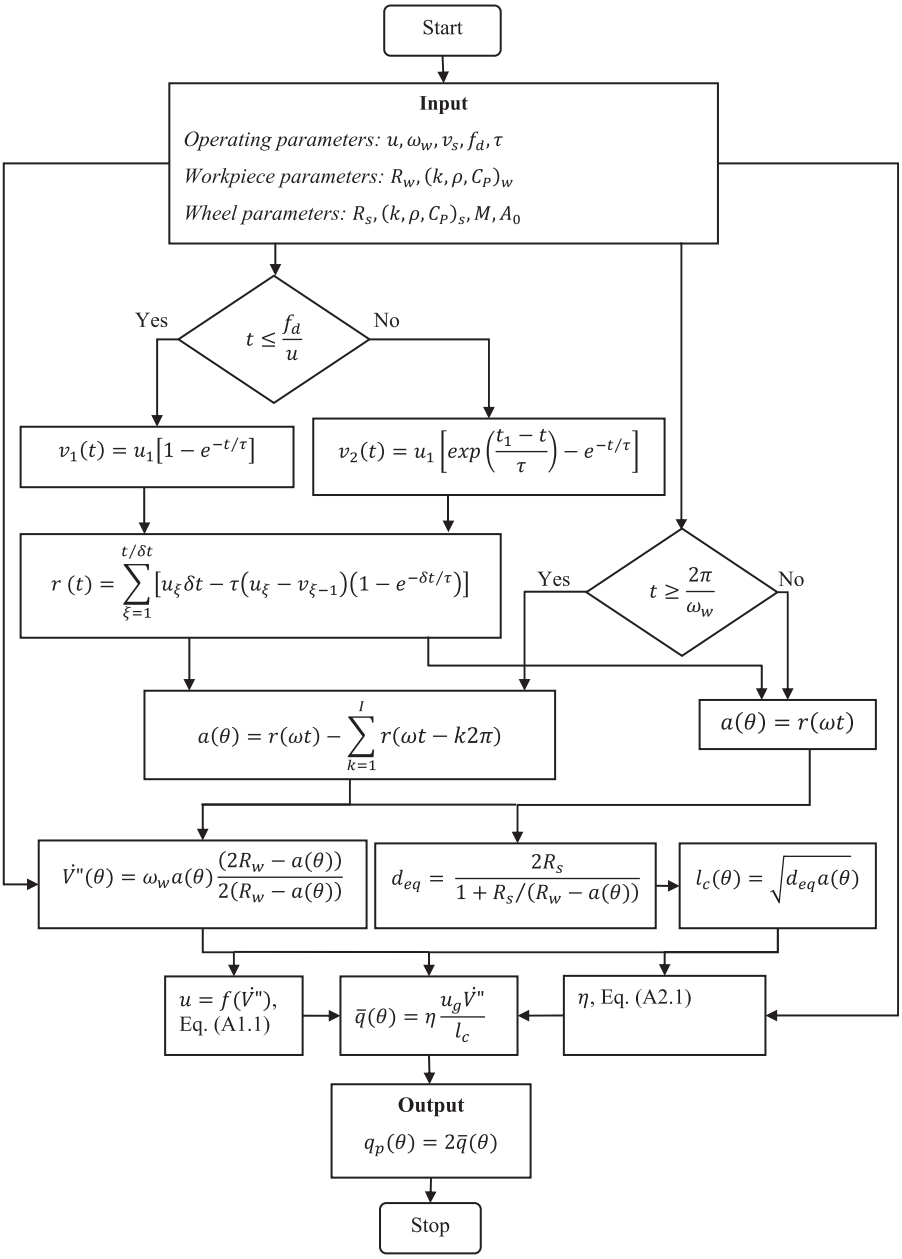

Fig. 3. Chart of calculating $q_p(\theta)$.

(b) For the second stage of ($t \geq t_1$ in associated with the spark-out where ($\theta \geq \theta_d$) where $u(t)=u_2=0$, the condition of continuity is $v_2(t_1)=u_1[1-e^{-t_1/\tau}]$ to which

$$v_2(t)=u_1\left[exp\left(\frac{t_1-t}{\tau}\right)-e^{-t/\tau}\right] \tag{22}$$

For a constant controlled feed rate, the discrete value of actual infeed δr between two consecutive sampling instants can be determined as [24]

$$\delta r=u_\xi \delta t-\tau(u_\xi-v_{\xi-1})(1-e^{-\delta t/\tau}) \tag{23}$$

It is therefore,

$$r(t)=\sum_{\xi=1}^{t/\delta t}[u_\xi \delta t-\tau(u_\xi-v_{\xi-1})(1-e^{-\delta t/\tau})] \tag{24}$$

On the other hand, as shown in Fig. 2, the workpiece will be loaded (I) times of cycles to complete the operation. The actual depth of cut in respect to time (t) after (k) cycles becomes

$$\begin{cases} a(t)=r(t), & t<\frac{2\pi}{\omega_w} \\ a(t)=r(t)-\sum_{k=1}^{I} r\left(t-k\frac{2\pi}{\omega_w}\right), & t\geq\frac{2\pi}{\omega_w} \end{cases} \tag{25a, b}$$

Since $\omega_w=const$ and from Eq. (18a), the actual depth of cut in respect to the angular position (θ) after (k) cycles on the workpiece can be rewritten as

$$\begin{cases} a(\theta)=r(\omega t), & t<\frac{2\pi}{\omega_w} \\ a(\theta)=r(\omega t)-\sum_{k=1}^{i} r(\omega t-k2\pi), & t\geq\frac{2\pi}{\omega_w} \end{cases} \tag{26a, b}$$

The grinding heat generated at location θ can therefore be calculated following the chart shown in Fig. 3.

2.3. Prediction of the hardened layer thickness

In a grinding-hardening process, the development of a hardened layer in a workpiece is a result of phase transformations in which the steel is heated above the Ac3 temperature. According to Refs. [25–27], by rapid heating, the transformation time of pearlite to austenite can be reduced. For instance, with the heating rate of 10^4 K/s as in laser hardening, the transformation time is only about 10 ms. As shown in Part 3.2 of the grinding-hardening results, the heating rate is very high, about 1.6×10^4 K/s, and the dwell time is about 10–30 ms. These are sufficient conditions for a complete austenite transformation. Therefore by probing the peak temperature developed at the Ac3 (770 °C for steel 1045) at subsurface distance of the workpiece, thickness of the hardened layer at an instant location, δ (θ, t), can be determined. However, as analysed in Section 2.2, in plunge cylindrical grinding, the workpiece will be loaded (I) times to complete the operation. A hardened layer thickness developed at a cycle ($k-1$) will be reduced when passing the next cycle, i.e., cycle (k), by the depth of cut (a_k) at that cycle. Depending on the probed thickness of the hardened layer developed at the kth cycle (δ_k), the actual hardened layer thickness developed after the k cycles (Δ_k) will vary, as illustrated in Fig. 4. Since the depth of cut is very much smaller than the workpiece radius ($a(\theta,t)\ll R_w$), it is reasonable to assume that the temperature developed on a workpiece with radius R_w is similar to that of radius [R_w–$a(\theta,t)$]. The hardened layer thickness (Δ_k) developed at the θ position, therefore, can be determined by

$$\Delta_k=\begin{cases} \delta_{k-1}-a_k, & \delta_{k-1}-a_k\geq\delta_k \\ \delta_k, & \delta_{k-1}-a_k<\delta_k \end{cases} \tag{27}$$

where $I\geq k\geq 2$.

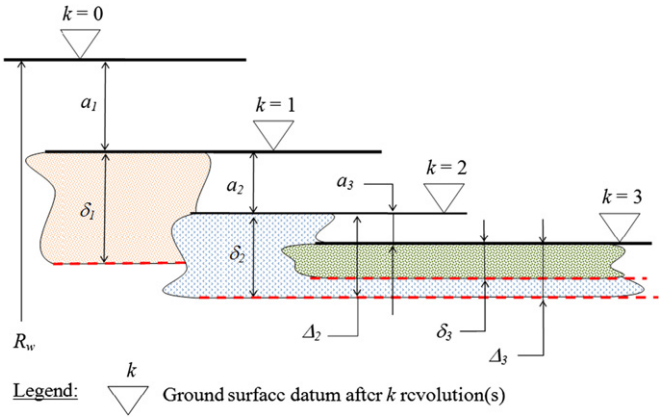

Fig. 4. Development of hardened layer thickness.

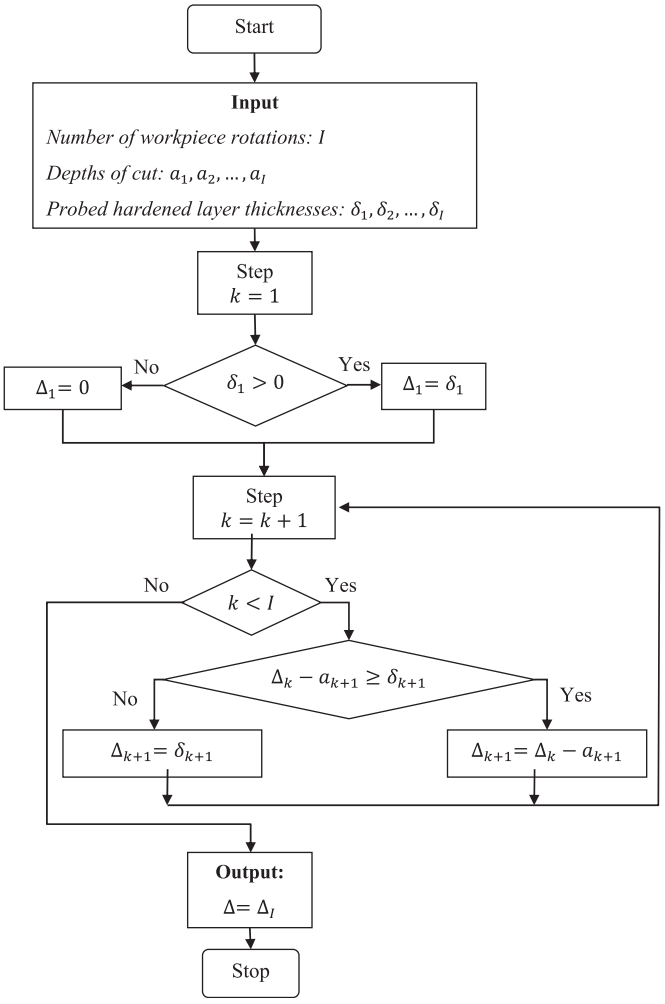

Fig. 5. Chart of calculating the hardened layer thickness Δ.

For the next step ($k+1$), δ_k is replaced by $\delta_k=\Delta_k$

$$\Delta_{k+1}=\begin{cases} \Delta_k-a_{k+1}, & \Delta_k-a_{k+1}\geq\delta_{k+1} \\ \delta_{k+1}, & \Delta_k-a_{k+1}<\delta_{k+1} \end{cases} \tag{28}$$

The final hardened layer thickness (Δ_I) is computed until reaching the last cycle I, following the chart shown in Fig. 5.

3. Verification

3.1. Experiment

Experiments were conducted using a Jones–Shipman cylindrical grinding machine. Grinding conditions are shown in Table 1. A workpiece was marked for determining the position of its initial engagement with the grinding wheel. Temperature rise in the workpiece was measured using a slipping device shown in Fig. 6. Wires of type K-thermocouple with a diameter of 0.127 mm and time constant of 0.05 s [28] were guided inside the workpiece to the surface to be ground where their junctions were embedded. The size of the thermocouples was selected so that it was large enough to withstand the mechanical stress during grinding and to cope with the rapid temperature fluctuation in grinding. The leads from the thermocouple wires were connected to pairs of pins rotated with the workpiece. The pins traced on a flat panel made from a printed circuit board (PCB) consisted of concentric and electrically insulated copper rings. The panel was attached on a fixed block made of electrically insulated Teflon where the thermocouple wires were led to a measuring system. The wires were metal-shielded for eliminating signal noise. A data acquisition (DAQ) system equipped with a high frequency response DAQ board, NI SCXI-1600 (sampling rate of 200 kS/s), a signal conditioning module, SCXI-1102B (high band width of 200 Hz) and an isothermal terminal block, SCXI-1303, was used. The data was collected and analysed using the *Labview* (*Laboratory Virtual Instrumentation Workbench*) programme. To inspect the hardened layer, the ground workpiece were sliced, polished and then etched using a solution of Nital containing 5% nitric acid and 95% ethanol by volume. The etched samples were inspected on a digital microscope, Keyence VHX-100. Hardness of the sample was measured using a hardness tester, Shimadzu Seisakusho NT-M00. Residual stresses were measured on an MSF-3M X-ray stress analyser (Rigaku Co., Japan), using the iso-inclination method. Since grinding-hardening experiments were conducted in atmospheric dry air, a scaling layer containing surface defects caused by the oxidation occurred on the surface of the ground workpieces [2]. To measure the residual stresses, it is necessary to retreat the sample surface after grinding-hardening. A second set of experiment was done to remove the scaling layer using a light grinding with a small total infeed of 10 μm [29] under significant coolant application. In this light grinding, the grinding wheel was dressed by a single diamond grit at a total dressing depth of 10×25 μm.

Table 1
Experimental conditions.

Grinding wheel	• Alumina, 57A60LV, diameter/width (mm/mm)=290/20. • Thermal properties at 300 K: k ($Wm^{-1}K^{-1}$)=46, ρ ($kg\,m^{-3}$)=3970, C_p ($Jkg^{-1}\,K^{-1}$)=770. • Wheel speed, ω_s (rpm): 1750 (26.6 m/s).
Workpiece	• Plain carbon steel 1045, diameter/width (mm/mm)=40/15. • Work speed, ω_w (rpm): 45 ± 1.0. • Controlled infeed rate, u_1 (mm/rev): 0.127 (0.085 mm/s) and 0.254 (0.169 mm/s). • Designed total infeed, f_d (μm): 200.

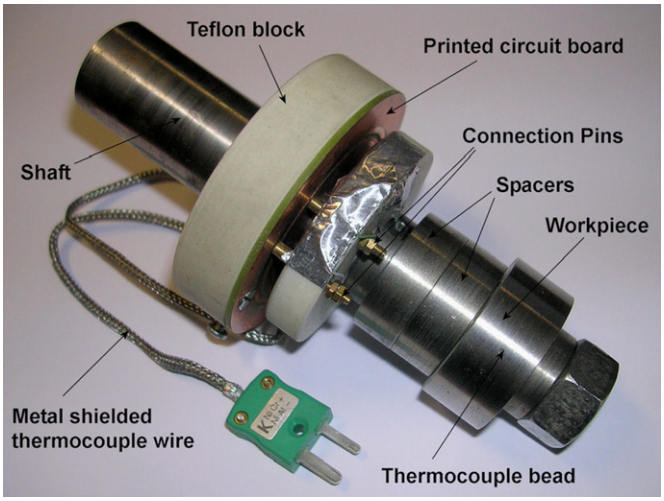

Fig. 6. Slipping device for measuring temperature.

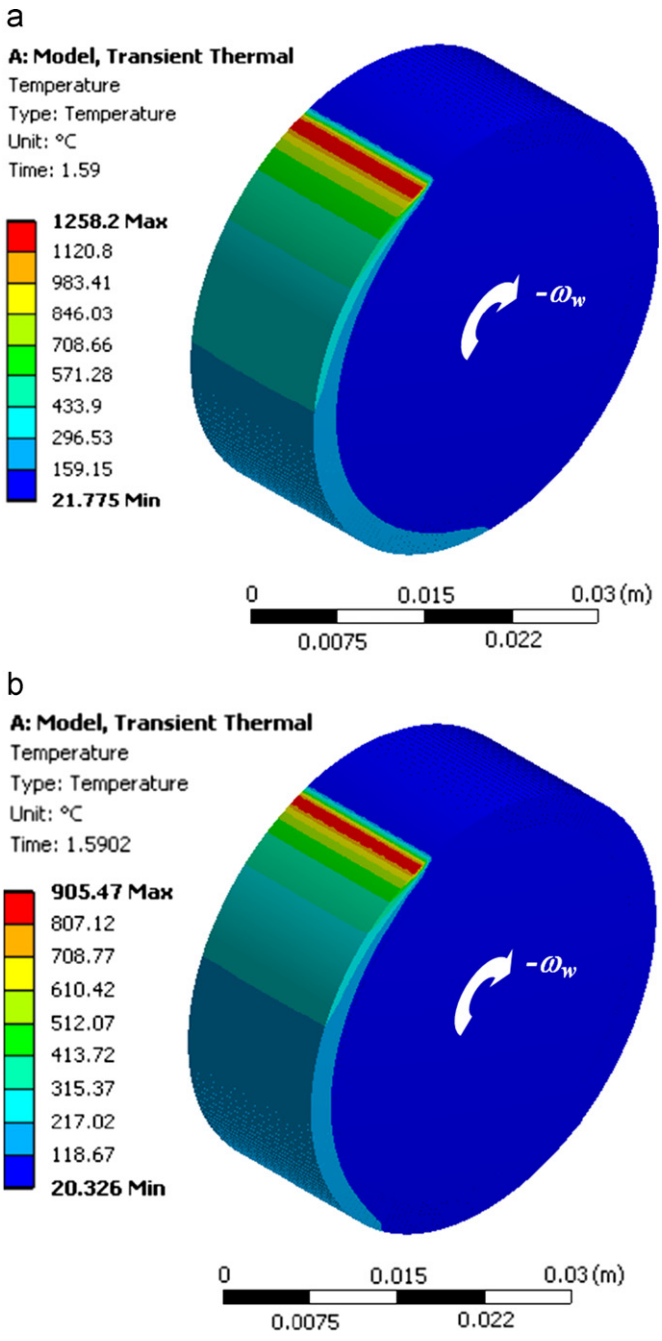

Fig. 7. Temperature field developed in the workpiece ground with different conditions: (7a) $\theta_d(=\omega_w f_d/u_1) < 2\pi$, $\theta_d = 0.787 \times 2\pi$, ($u_1 = 0.254$ mm/rev) and (7b) $\theta_d > 2\pi$, $\theta_d = 1.574 \times 2\pi$, ($u_1 = 0.127$ mm/rev).

3.2. Results and discussion

Fig. 7 shows the simulation result of the temperature field developed in the workpiece. When the heat source moved along the workpiece surface, the highest temperature rise was within the wheel–workpiece contact zone. At any instant position θ, the temperature reached its maximum in the surface and reduced with the subsurface distance. A higher infeed rate resulted in a greater temperature rise (Fig. 7a), due to the higher grinding heat generated at a greater material removal rate.

Fig. 8 shows the temperature history developed on the ground surface during grinding. The deviation between the theoretical and experimental peak values was within 11.5–28.3%, which is reasonable when the thermocouple technique is used [30,31]. The discrepancy was mainly due to the time lag in dynamic response of thermocouples within a small period of time [32], because the time constant of the thermocouples used in this study was 0.05 s, larger than the minimum time step in the transient heat transfer of 0.004 s in the finite element simulation. Hence, the theoretical predictions were verified by the experimental measurements.

The results show that the instant depth of cut varies and that the heating and cooling processes repeat. The number of the heating–cooling cycles and the magnitude of the heat flux depend on the ratio ($\theta_d = \omega_w f_d / u_1$). For instance, at the position III of the workpiece ground with $\theta_d < 2\pi$, $u_1 = 0.254$ mm/rev (Fig. 8a), the grinding operation completes after 2 workpiece revolutions ($I = 2$) during which the temperature necessary for the austenising in the steel (Ac3) is reached at the second revolution, i.e. 1142 °C. It is followed by a rapid quenching (about 4000 K/s) to temperature Ms with the dwell time of 12 ms, which enables martensite transformation [25–27]. If a workpiece is ground at a lower infeed rate (e.g., $\theta_d > 2\pi$, $u_1 = 0.127$ mm/rev as shown in Fig. 8b), the martensitic transformation also takes place at the second workpiece revolution, but at a lower degree of the peak temperature (934 °C). In this case, the grinding operation will complete after 3 workpiece revolutions ($I = 3$). The workpiece surface after the martensitic transformation will experience a tempering process due to the reheating at the peak temperature of 586 °C when $k = 3$. It is noted that due to the workpiece rotation, different workpiece positions experience different heating and cooling cycles. The highest peak temperature (1205 °C at $k = 2$) and surface tempering (408 °C at $k = 3$) occur at Position II when the workpiece is ground at the infeed rate of $u_1 = 0.254$ mm/rev. At the last revolution of completing the grinding operation, reheating to a temperature above Ac3 takes place at Positions I (1007 °C) and IV (872 °C), leading to another martensitic transformation process. When grinding is conducted at the lower infeed rate of $u_1 = 0.127$ mm/rev; however, the highest peak temperature appears at Position IV (947 °C at $k = 2$) and surface tempering is at Position III (586 °C at $k = 3$). The repeated martensitic transformation only occurs at Position II (822 °C at $k = 3$).

The above variation of heating and cooling affects the generation of the hardened layer. Fig. 9 shows the hardened layer thickness and surface residual stresses obtained at different circumferential positions on the ground workpieces. The hardness distributions were shown in Fig. 10. The average hardness of the hardened layers was 707 HV(500 g load), higher hardness than that can be obtained from an ordinary quenching (560 HV) [2] and from the core part of the 1045 steel samples without hardening ($\approx$ 250 HV). Residual stresses ($\sigma_{\theta\theta}$) were measured in the direction

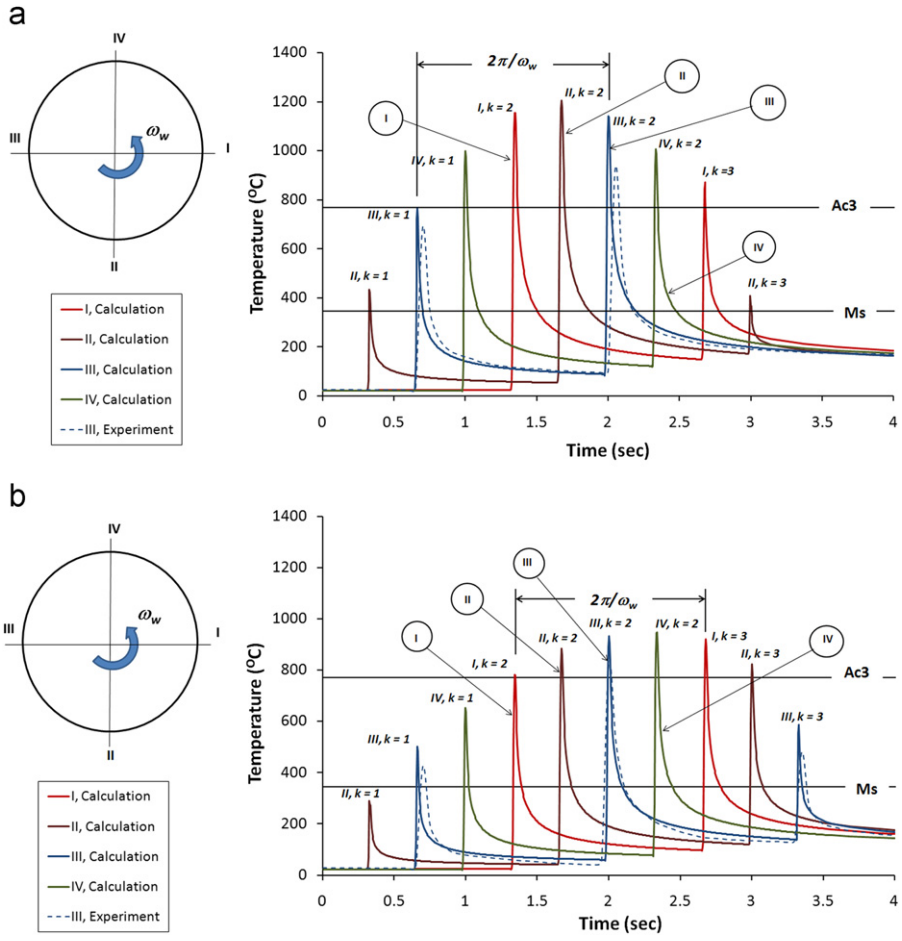

Fig. 8. Temperature history in the workpiece surface ground with different operating conditions: (8a) $\theta_d (= \omega_w f_d / u_1) < 2\pi$, $\theta_d = 0.787 \times 2\pi$, ($u_1 = 0.254$ mm/rev) and (8b) $\theta_d > 2\pi$, $\theta_d = 1.574 \times 2\pi$, ($u_1 = 0.127$ mm/rev).

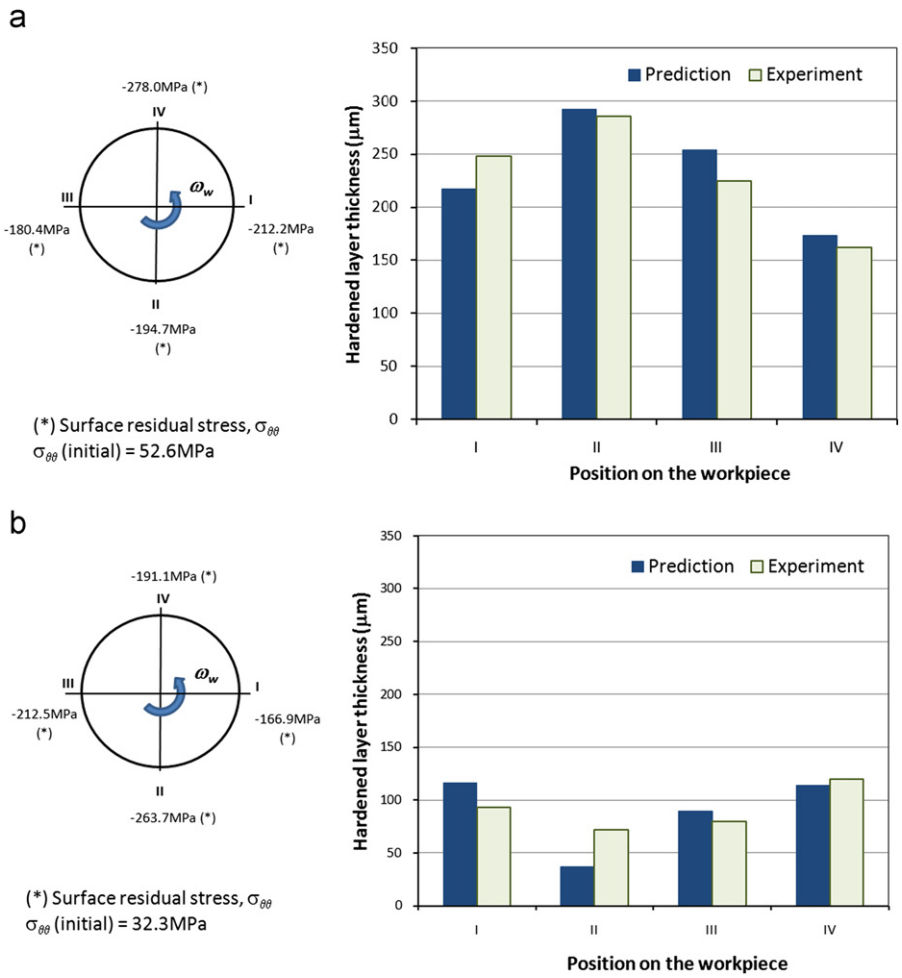

Fig. 9. Prediction of the hardened layer thickness and measured residual stresses, (9a) $\theta_d(=\omega_w f_d/u_1)<2\pi$, $\theta_d=0.787\times 2\pi$, ($u_1=0.254$ mm/rev) and (9b) $\theta_d>2\pi$, $\theta_d=0.574\times 2\pi$, ($u_1=0.127$ mm/rev).

tangential to the workpiece circumference and the measurements on the surface of the samples prior to grinding with $u_1=0.254$ mm/rev and $u_1=0.127$ mm/rev were 52.6 and 32.3 MPa, respectively. Induced compressive residual stresses were found on different positions of the workpiece surface after grinding-hardening, varying from -184.4 to -278.0 MPa ($u_1=0.254$ mm/rev) and from -166.9 to -263.7 MPa ($u_1=0.127$ mm/rev). Highest compressive stresses were found at Position IV (-278.0 MPa) of the workpiece ground with $u_1=0.254$ mm/rev and at Position II (-263.7 MPa, $u_1=0.254$ mm/rev), where they experienced the repeated martensitic transformation process. Heavy and repeated loading in grinding-hardening causes a high degree of plastic deformation as typically shown in Fig. 11. It is revealed that the alteration of microstructure due to the combination effect of phase transformation and mechanical stresses results in an enhancement of layer hardness and beneficial compressive residual stresses [2,4,5].

The hardened layer thickness distributed on the workpiece circumference is not uniform and varies from 173.3 to 292.4 μm (234.3 μm in average) in the workpiece ground at the speed of $u=0.254$ mm/rev, but from 37 to 116 μm (89.2 μm in average) in that ground at $u=0.127$ mm/rev. This means that a higher hardened thickness is obtained at a lower ratio ($\theta_d=\omega_w f_d/u_1$). This is mainly due to two reasons. First, under a higher infeed rate, the material removal rate is greater and hence the material volume, which can be heated to above the phase transformation temperature Ac3, is larger. Secondly, as analysed in Section 2.3, the hardened layer thickness developed at cycle $(k-1)$ will be reduced during the following cycle (k). To complete a given designed total infeed, a lower infeed rate requires a greater number of revolutions. As a result, the hardened layer thickness becomes smaller.

Nevertheless, it is worthwhile noting that although grinding at a higher infeed rate can produce a thicker hardened layer, a too high speed may lead to an unstable process and requires a high powered machine. At a certain level of material removal rate, grinding heating can melt the surface material of the workpiece. Because grinding-hardening is a dry process, no coolant is used for the cleaning of the clogging chips loaded to wheel pores [33], leading to an accelerated wheel wear and unexpected degradation of dimensional accuracy of a ground component. A further study will be conducted for optimising the balance between the demands in the thickness of beneficially microstructural layer and the cost of the process due to the instability.

The comparison of the theoretical results with the experimental measurements clearly shows that grinding-hardening in plunge cylindrical grinding is feasible and controllable. The hardened thickness and its variation are predictable by the model developed.

4. Conclusions

A temperature-dependent heat transfer model incorporating the moving heat source has been developed to predict the temperature fields and the consequent thickness of the hardened layer in plunge cylindrical grinding. The model was experimentally verified on

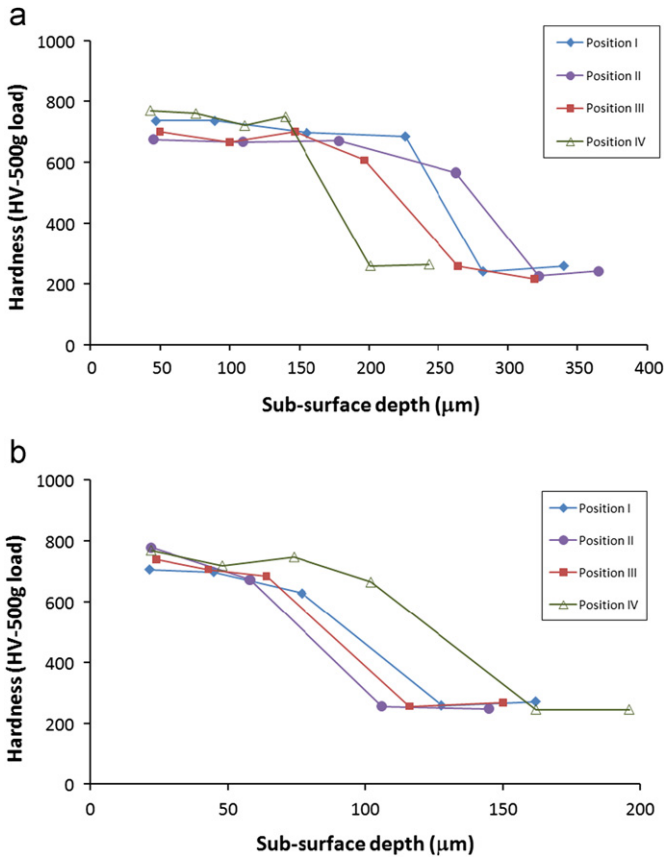

Fig. 10. Hardness distribution on the hardened layers. (a) $\theta_d = 0.787 \times 2\pi$, ($u_1 = 0.254$mm/rev) and (b) $\theta_d = 1.574 \times 2\pi$, ($u_1 = 0.127$ mm/rev).

quenchable steel 1045. The model provides a fundamental insight into the heat transfer mechanism in grinding-hardening, which can be used for further studying the optimisation and control of the process. Specifically, the following findings are particularly useful:

(1) The ratio of the workpiece rotation speed to the infeed rate of the grinding wheel plays an important role in the heat treatment cycle of the hardened surface layer. Grinding at a higher infeed rate produces a thicker hardened layer, and *vice versa*. However, a too high speed may cause an unstable process.
(2) The heating cycle in plunge cylindrical grinding is the result of consecutive heating and cooling processes, varying from location to location in a workpiece. The phase transformation under mechanical stresses in grinding-hardening results in a hardened layer with hardness enhancement and beneficial compressive residual stresses.

Acknowledgement

This project was financially supported by the Australian Research Council (ARC).

Appendix

A1. Specific grinding energy

The calculation of specific grinding energy is based on the empirical relationship:

$$u_g = 61.64\dot{V}''^{-0.176} \quad \text{(A1.1)}$$

where the units of u_g and $\dot{V}''$ used in Eq. (A1.1) are J/mm^3 and mm^3/(ms), respectively. The correlated data were the nominal values obtained from experiments conducted at various specific material removal rates conducted by Heinzel and Bleil [18], Marinescu et al. [19] and Fricker et al. [17] (Fig. 12), of which the grinding conditions are described in Table 2.

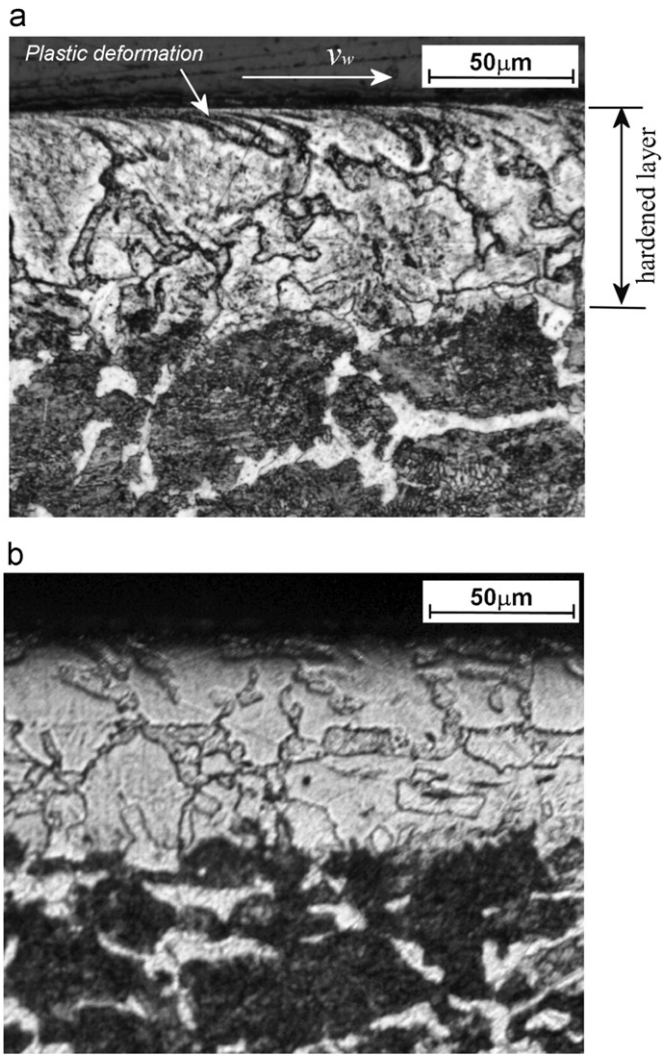

Fig. 11. Plastic deformation in the hardened layer at Position III ($u = 0.127$ mm/rev). (a) in the (r, θ) plane and (b) in the (r, z) plane.

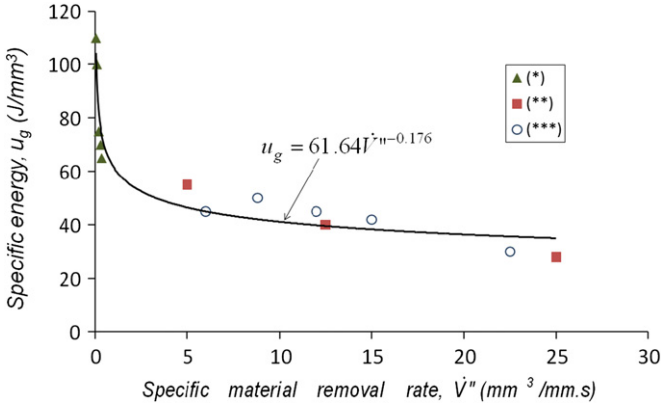

Fig. 12. Specific energy versus specific material removal rate: (*) Heinzel and Bleil [18], (**) Marinescu et al. [19] and (***) Fricker et al. [17].

Table 2
Grinding conditions in the experiments to determine the specific grinding energy.

	Grinding wheel/workpiece material	Specific material removal rate, u_g (mm^3/mm s)
Heinzel and Bleil [18]	EKW150V2B/AISI 4140 steel	0.05–0.35
Marinescu et al. [19]	Alumina/hardened carbon steel	5.0–25.0
Fricker et al. [17]	CBN/ AISI 4140 steel	6.0–22.5

A2. Heat partition ratio

The heat partition ratio (η) can be determined according to the analysis of burn prediction [34]:

$$\eta = \left\{1+1.06\left[\frac{(k\rho C_p)_s v_s}{(k\rho C_p)_w v_w}\right]^{0.5} f(\xi)A_0 G_a\right\}^{-1} \quad \text{(A2.1)}$$

where function $f(\xi)$ takes into account the fact that the cross-section area of the wheel grain is substantially higher than the contact area between the wheel grain and the workpiece and is given by [35]

$$f(\xi) = \frac{2}{\pi^{0.5}}\frac{\xi}{1-exp(\xi^2)erf(\xi)} \quad \text{(A2.2)}$$

$$\xi = \left(\frac{\gamma\pi\alpha_s l_c}{2A_0 v_s}\right)^{0.5} \quad \text{(A2.3)}$$

In Eqs. (A2.1)–(A2.3), the subscripts s and w denote the wheel-grain and the workpiece, respectively; γ is an abrasive shape factor and is taken to be unit since grains used in making the grinding wheels are approximately equiaxed [31]; A_o is the average single grain-workpiece contact area corresponding to the truncated cone; and G_a is the number of active grains per unit area of the wheel surface.

The thermal properties of the grinding wheel and workpiece materials used in this calculation are considered at 300 K as shown in Table 1 [36] and from Ref. [11], respectively.

The average single grain-workpiece contact area A_o can be approximated as 5% of the projected grain area ($\pi d_g^4/4$) [35], where the grain size (d_g) is computed by [23]

$$d_g(\text{mm}) = 64M^{-1.4} \quad \text{(A2.4)}$$

where M is the manufacturing grit number (i.e., M=60 for the wheel used in this study)

The number of active grains per unit area of the wheel surface (G_a) is calculated as:

$$G_a = \frac{V_p}{(\pi d_g^2/4)} \quad \text{(A2.5)}$$

where V_p is the volumetric packaging density of grains in the wheel constituent, taken as 40% for the aluminium oxide wheel used [23].

For the experimental parameters given in Table 1, the heat partition ratio calculated is in the range of 38–68%. These values are in agreement with other works [35] that fall in the range of 60–75% for the use of aluminium oxide wheel.

A3. Heat transfer coefficient

The heat transfer coefficient, h_a, is estimated following the Hilbert's empirical relation for a circular cylinder with radius R_w subjected to a cross flow of air [12,37].

$$Nu = \frac{2h_a R_w}{k_a} = CRe^m Pr^{1/3} \quad \text{(A3.1)}$$

$$\begin{cases} 4\times10^3 < Re < 4\times10^4 : C = 0.193, \quad m = 0.618 \\ 4\times10^4 \le Re < 4\times10^6 : C = 0.027, \quad m = 0.805 \end{cases}$$

where k_a is the thermal conductivity of air; Nu, Pr and Re are the Nusselt, Prandtl and Reynolds numbers, respectively. The flow of air is induced by the relative motion of the wheel, thus Re can be defined as

$$Re = \frac{2v_s R_w}{\upsilon} \quad \text{(A3.2)}$$

where υ is the viscosity of air.

The thermal properties of air (k_a, υ and Pr) are functions of temperature and are considered at the film temperature, T_f=0.5(T_s+T_∞). For the given grinding conditions in Table 1, the dependency of heat transfer coefficient on the wall surface temperature within the range of 22 °C (ambient temperature) to 1495 °C (melting temperature of the workpiece material) is computed by

$$h_a = 187.3(T_s + T_\infty)^{-0.128} \quad \text{(A3.3)}$$

where h_a is in W/m^2 K, T_w and T_∞ are in Celsius degree and T_∞=22 °C (inititial condition).

References

[1] E. Brinksmeier, T. Brockhoff, Utilization of grinding heat as a new heat treatment process, CIRP Annals—Manufacturing Technology 45 (1) (1996) 283–286.
[2] T. Nguyen, I. Zarudi, L.C. Zhang, Grinding–hardening with liquid nitrogen: mechanisms and technology, International Journal of Machine Tools and Manufacture 47 (1) (2007) 97–106.
[3] L. Zhang, Grinding–hardening of steel surfaces: a focused review, International Journal of Abrasive Technology 1 (1) (2007) 3–36.
[4] I. Zarudi, L.C. Zhang, Mechanical property improvement of quenchable steel by grinding, Journal of Materials Science 37 (18) (2002) 3935–3943.
[5] I. Zarudi, L.C. Zhang, Modelling the structure changes in quenchable steel subjected to grinding, Journal of Materials Science 37 (20) (2002) 4333–4341.
[6] H. Bhadeshia, Bainite in Steels—Transformations, Microstructure and Properties., second ed., The University Press, Cambridge, 2001.
[7] L.C. Zhang, T. Suto, H. Noguchi, T. Waida, Applied mechanics in grinding, part III: a new formula for contact length prediction and a comparison of available models, International Journal of Machine Tools and Manufacture 33 (4) (1993) 587–597.
[8] I. Zarudi, L.C. Zhang, A revisit to some wheel–workpiece interaction problems in surface grinding, International Journal of Machine Tools and Manufacture 42 (8) (2002) 905–913.
[9] M. Mahdi, L.C. Zhang, Applied mechanics in grinding, part V: thermal residual stresses, International Journal of Machine Tools and Manufacture 37 (5) (1997) 619–633.
[10] M. Mahdi, L.C. Zhang, The finite-element thermal analysis of grinding processes by ADINA, Computers & Structures 2–3 (56) (1995) 313–320.
[11] T. Nguyen, L. Zhang, Grinding–hardening using dry air and liquid nitrogen: prediction and verification of temperature fields and hardened layer thickness, International Journal of Machine Tools and Manufacture 50 (10) (2010) 901–910.
[12] F.P. Incropera, D.P. Dewitt, Fundamentals of Heat and Mass Transfer, third ed., John Wiley & Sons Inc., 1990.
[13] Y. Nagasaka, J.K. Brimacombe, E.B. Hawbolt, I.V. Samarasekera, B. Hernandez-Morales, S.E. Chidiac, Mathematical model of phase transformations and elastoplastic stress in the water spray quenching of steel bars, Metallurgical Transactions A 24A (1993) 795–808.
[14] D.P. Koistinen, R.E. Marburger, A general equation prescribing the extent of the austenite–martensite transformation in pure iron–carbon alloys and plain carbon steels, Acta Metallurgica 7 (1) (1959) 59–60.

[15] S. Denis, D. Farias, A. Simon, Mathematical model coupling phase transformations and temperature evolutions in steels, ISIJ International 32 (3) (1992) 316–325.
[16] C. Verdi, A. Visintin, A mathematical model of the austenite–pearlite transformation in plain carbon steel based on the Scheil's additivity rule, Acta Metallurgica 35 (11) (1987) 2711–2717.
[17] D.C. Fricker, T.R.A. Pearce, A.J.L. Harrison, Predicting the occurence of grind hardening in cubic boron nitride grinding of crankshaft steel, Proceedings of the Institution of Mechanical Engineers, Part B: Journal of Engineering Manufacture 218 (2004) 1339–1356.
[18] C. Heinzel, N. Bleil, The use of the size effect in grinding for work-hardening, Annals of the C.I.R.P. 56 (1) (2007) 327–330.
[19] I. Marinescu, M. Hitchiner, E. Uhlmann, W.B. Rowe, I. Inasaki, Handbook of Machining with Grinding Wheels, Taylor & Francis Group, CRC Press, 2007.
[20] M.C. Shaw, Principles of Abrasive Processing, Oxford University Press, 1996.
[21] S. Malkin, Y. Koren, Optimal infeed control for accelerated spark-out in plunge grinding, Journal of Engineering for Industry, Transactions of the ASME 106 (1984) 70–74.
[22] S. Malkin, Grinding of metals: theory and application, Journal of Applied Metal Working 3 (2) (1984) 95–109.
[23] S. Malkin, C. Guo, Grinding Technology—Theory and Applications of Machining with Abrasives, second ed., Industrial Press, 2008.
[24] S. Dong, K. Danai, S. Malkin, A. Deshmukh, Continuous optimal infeed control for cylindrical plunge grinding, part 1: Methodology, Journal of Manufacturing Science and Engineering 126 (2004) 327–333.
[25] E. Ohmura, K. Inoue, K. Haruta, Computer simulation on structural changes of hypoeutectoid steel in laser transformation hardening process, JSME International Journal, Series 1: Solid Mechanics, Strength of Materials 32 (1) (1989) 45–53.
[26] H. Eda, E. Ohmura, S. Yamauchi, I. Inasaki, Computer visual simulation on structural changes of steel in grinding process and experimental verification, CIRP Annals—Manufacturing Technology 42 (1) (1993) 389–392.
[27] G.N. Haidemenopoulos, Coupled thermodynamic/kinetic analysis of diffusional transformations during laser hardening and laser welding, Journal of Alloys and Compounds 320 (2) (2001) 302–307.
[28] 〈http://www.omega.com/temperature/Z/pdf/z051.pdf〉.
[29] T. Nguyen, L.C. Zhang, An assessment of the applicability of cold air–oil mist in surface grinding, Journal of Materials Processing Technology 140 (1-3) (2003) 224–230.
[30] R. Snoeys, M. Maris, J. Peters, Thermally induced damage in grinding, Annals of the C.I.R.P. II (1978) 571–581.
[31] C. Guo, Y. Wu, V. Varghese, S. Malkin, Temperatures and energy partition for grinding with vitrified CBN wheels, Annals of the C.I.R.P. 48 (1) (1999) 247–250.
[32] J.W. Dally, W.F. Riley, K.G. McConnell, Instrumentation for Engineering Measurements, second ed., John Wiley & Sons, Inc., 1993.
[33] T. Nguyen, L.C. Zhang, Performance of a new segmented grinding wheel system, International Journal of Machine Tools and Manufacture 49 (3–4) (2009) 291–296.
[34] C. Guo, S. Malkin, Heat transfer in grinding, Journal of Materials Processing and Manufacturing Science 1 (1) (1992) 16–27.
[35] S. Kohli, C. Guo, S. Malkin, Energy partition to the workpiece for grinding with aluminium oxide and CBN abrasive wheels, Transactions of the ASME 117 (1995) 160–168.
[36] A.S. Lavine, A simple model for convective heat transfer during the grinding process, Journal of Engineering for Industry 110 (1988) 1–6.
[37] M. Jakob, Heat Transfer, vol. 1, Wiley, New York, 1949.